

Nonlinear generation of quantum-entangled photons from high- Q states in dielectric nanoparticles

Alexander N. Poddubny^{1,2,*} and Daria A. Smirnova^{2,3}

¹*Ioffe Institute, St. Petersburg 194021, Russia*

²*Nonlinear Physics Centre, Australian National University, Canberra ACT 2601, Australia*

³*Institute of Applied Physics, Russian Academy of Science, Nizhny Novgorod 603950, Russia*

We develop multipolar theory of nonlinear generation of entangled photons from subwavelength dielectric particles due to the spontaneous parametric downconversion. We demonstrate that optical excitation in resonance with the high-quality supercavity mode of the aluminum gallium arsenide (AlGaAs) nanodisk leads to a strong enhancement of generation of entangled photon pairs associated with electric and magnetic dipole modes. Our rigorous numerical results are corroborated by an analytical model, universally describing formation of high- Q resonant states and dark states due to the interference and interplay of the parent multipoles, namely, magnetic dipoles and magnetic octupole. Our findings and description can be instructive for quantum and nonlinear nanophotonics applications.

I. INTRODUCTION

Quantum communications and information processing technologies demand for compact emitters of entangled photons [1, 2]. Despite the recent advances with the quantum dot setups [3, 4], so far the spontaneous wave mixing in nonlinear crystals remains the most efficient approach for room-temperature two-photon generation [5, 6]. However, bringing efficient and integrable quantum nonlinear emitters to the nanoscale is quite challenging. A promising recently emerged versatile platform to enhance nonlinear processes is based on semiconductor nanoparticles, such as Si and AlGaAs, supporting pronounced Mie-type resonances and possessing strong optical nonlinearities [7]. So far most of the studies have been focused on enhancement of classical nonlinear processes, including second-harmonic [8, 9], sum-frequency and third harmonic [10–12] generation. While initial experiments on the nonlinear entangled photon generation from AlGaAs nanoantennas are already available [13, 14], fundamental and complementary design approaches are still required to improve the modes quality and the resulting generation efficiency.

Recently it has been suggested to utilize so-called high-quality (high- Q) resonant states to enhance the simplest classical nonlinear process of second-harmonic generation in dielectric nanodisks [15]. These states are akin to the bound states of continuum (BICs) in infinite periodic dielectric structures [16]: their high finesse is due to the destructive interference of several far-field radiation channels [17, 18]. However, the multipolar nature of such high- Q resonant states and their potential for applications in quantum nanophotonics have not yet been studied.

Here we put forward the high- Q resonant states for the enhanced generation of entangled photons by spontaneous parametric downconversion (SPDC) in the nan-

odisk with the bulk quadratic nonlinearity $\chi^{(2)}$. Our calculation reveals an enhancement of generation of entangled photons in electric and magnetic dipole modes when a sum of their frequencies is equal to that of the high- Q state. Our model is based on the general rigorous Green-function-based quantum-optical theory for two-photon generation in arbitrary nonlinear nanostructures we recently developed [19, 20]. We also propose a fully analytical 3-level model that provides useful insights in the formation of resonant states. Explicit account for the two magnetic quasi-dipole modes and one magnetic quasi-octupole mode generalizes the previous 2-state approaches [17, 18] and allows us a universal simultaneous description of high- Q states and dark states in the multipolar scattering of dielectric nanodisks. It might also be useful to describe the characteristic Fano features in the optical scattering spectra [18].

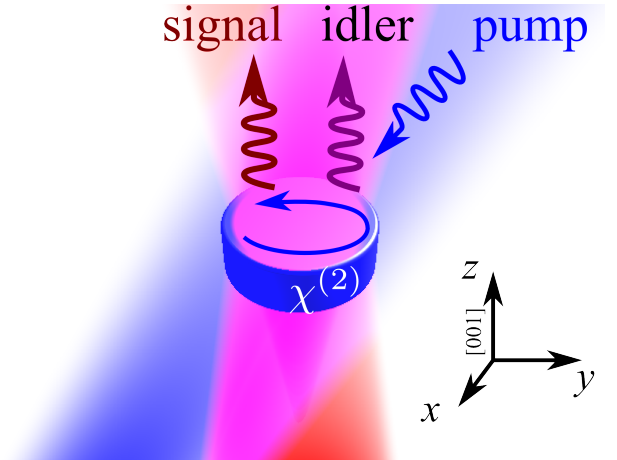


FIG. 1. Schematic of the entangled photons generation from a nonlinear nanodisk. TE-polarized plane wave pump excites a hybridized quasi-magnetic dipole-octupole high- Q state with angular momentum projection $M = 0$. The signal and idler photons are in in-plane electric and magnetic quasi-dipole modes.

* poddubny@coherent.ioffe.ru

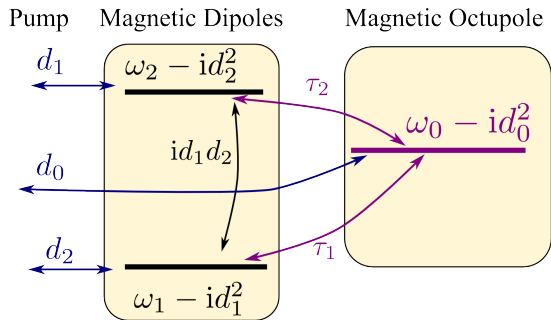


FIG. 2. Schematic of the three-level model for the formation of dark and high-Q state, captured by the Hamiltonian Eq. (4).

II. LINEAR MULTIPOLAR SCATTERING

The scheme of the structure under consideration is shown in Fig. 1. We consider a semiconductor nanodisk in air with the permittivity ε and nonlinear susceptibility $\chi^{(2)}$, oriented along the z axis. Our numerical approach is based on the t -matrix or extended boundary condition method [21–23]. Namely, the electric field is expanded over the vector spherical harmonics in the following way:

$$\mathbf{E}(\mathbf{r}) = \begin{cases} \sum_{\nu} [a_{0,\nu} \mathbf{J}_{\nu}(k_{\text{out}} \mathbf{r}) + a_{\text{scat},\nu} \mathbf{H}_{\nu}(k_{\text{out}} \mathbf{r})], & (\text{air}) \\ \sum_{\nu} a_{\text{in},\nu} \mathbf{J}_{\nu}(k_{\text{in}} \mathbf{r}), & (\text{disk}) \end{cases} \quad (1)$$

outside and inside the disk, respectively. Here the index ν incorporates the total angular momentum J , its projection to z axis M and the polarization $\sigma = \text{TE, TM}$; $k_{\text{out}} = \omega/c$ and $k_{\text{in}} = \omega\sqrt{\varepsilon}/c$. The functions \mathbf{J} and \mathbf{H} are regular and outgoing vector spherical harmonics [22]. The scattering is described by the Q and t matrices, linking the incident field with the field inside the disk and the scattered field,

$$a_{\text{in}} = Q^{-1} a_0, \quad a_{\text{scat}} = t a_0 \quad (2)$$

and related by

$$t = -i \text{Im} Q \cdot Q^{-1}. \quad (3)$$

While the numerical calculation of the t matrix is straightforward, it is instructive to study analytically how the interference between different multipolar modes manifests in the scattering.

Analytical 3-state model

In the case of spherical symmetry the t -matrix is diagonal. For cylindrical symmetry it remains diagonal in angular momentum projection M only, while the modes with different total momentum or polarization can hybridize. Specifically, the hybridization takes place between the modes with the same polarization and even

$J - J'$ as well as different polarization and odd $J - J'$. The high- Q resonant state, proposed in [17], corresponds to $M = 0$, when the TE and TM polarizations are decoupled. In order to elucidate its nature we put forward an analytical 3-level model, schematically illustrated in Fig. 2. Our consideration generalizes the approach developed in Ref. [24], describing the dark state in scattering by a mutual suppression of two scattering channels. Here we also include a third state and the resulting basis includes two quasi-magnetic-dipole states $|1\rangle, |2\rangle$ with $m = 0$, and first and second radial quantum numbers and the lowest quasi-magnetic-octupole state $|0\rangle$.

The non-Hermitian Hamiltonian of the structure assumes the form

$$H = \begin{pmatrix} \omega_1 - id_1^2 & -id_1 d_2 & \tau_1 \\ -id_1 d_2 & \omega_2 - id_2^2 & \tau_2 \\ \tau_1 & \tau_2 & \omega_0 - id_0^2 \end{pmatrix}. \quad (4)$$

The d coefficients are the effective dipole moments, governing both the radiative decay of the states and their coupling to the external field. The τ coefficients describe the hybridization of the dipole and octupole modes. Ohmic losses are neglected. The t -matrix in the basis of dipole and octupole channels, $D \equiv J = 1, M = 0, TE$ and $O \equiv J = 3, M = 0, TE$, is given by

$$t = iu(H - \omega)^{-1}u^T, \quad u = \begin{pmatrix} d_1 & d_2 & 0 \\ 0 & 0 & d_0 \end{pmatrix}, \quad (5)$$

where the u matrix describes the coupling of the incident field to the states 0, 1, 2. It is not quadratic since there exist two dipole modes and only one octupole mode. It is convenient to present the t -matrix in our model in the form Eq. (3), where the Q matrix reads

$$\text{Re} Q = \begin{pmatrix} -\frac{(\omega_1 - \omega)(\omega_2 - \omega)}{v_{DD}} & -\frac{v_{DD}}{d_0^2} \\ -\frac{v_{DO}}{d_0 v_{DD}} & \frac{d_0 v_{DO}}{\omega_0 - \omega} \end{pmatrix}, \quad (6)$$

$$\text{Im} Q = \begin{pmatrix} 1 & \frac{(d_1 t_2 - d_2 t_1)^2}{d_0 v_{DO}} \\ 0 & 1 \end{pmatrix}, \quad (7)$$

$$v_{DD} = (\omega_1 - \omega)d_2^2 + (\omega_2 - \omega)d_1^2, \quad (8)$$

$$v_{DO} = d_1 t_1 (\omega_2 - \omega) + d_2 t_2 (\omega_1 - \omega). \quad (9)$$

An explicit form of the t -matrix can be readily calculated from Eqs. (6)–(9). It fully satisfies the reciprocity and unitarity conditions $t^T = t, S^\dagger S = 1$ where $S = 1 + 2t$ is the scattering matrix. The advantage of the form Eqs. (6)–(9) is that it facilitates the extraction of the model parameters from the numerically computed Q -matrix. In that follows, we are most interested in the imaginary part of the eigenfrequency of the high- Q -state, that can be found from the position of the resonance of t_{OO} and reads

$$-\text{Im} \omega_O = d_0^2 + \frac{v_{DO}^2}{v_{DD}^2 + (\omega_1 - \omega)^2 (\omega_2 - \omega)^2}. \quad (10)$$

Two essential results of the model Eq. (6)–(10) are as follows. First, the dark state is formed in the dipole channel due to the destructive interference of first and second dipole modes in the far field, i.e. $v_{DD} = 0$ in Eq. (8) [24]. This means that the effective oscillator strength of the dipole transition vanishes and the dipolar scattering is quenched. Second result is the formation of the high-quality resonant state due to the destructive interference of first and second dipole modes in the coupling to the octupole mode, i.e. $v_{DO} = 0$. It is manifested as a suppression of the radiative losses in the octupole channel, Eq. (10). The effect can be also understood as a decoupling of the octupole mode from the dipole ones. The quality factor of the octupole resonance is intrinsically higher than that for the dipole in $(\lambda/L)^4$ times, where L is the characteristic disk size and λ is the wavelength. However, in the general case this quality factor is suppressed due to the hybridization with the dipole mode. If there were only one dipole mode, it would hybridize with the octupole one and increase its linewidth (second term in Eq. (10)). However, the presence of two dipole modes enables the mutual cancellation of the radiative damping and restores the intrinsically high finesse of the octupole resonance.

Figure 3 shows the dependence of the scattering spectra on the aspect ratio of the disk r/h . Results in the left and right columns are calculated numerically and agree with Ref. [17]. Right column has been calculated analytically using the parameters extracted from the numerically found Q -matrices. We note, that in the extraction procedure it is necessary to include a small admixture of the magnetic modes with $J = 5, 7$ to the octupole state. This means adding a correction $-Q_{\nu\nu_1}[Q^{-1}]_{\nu_1\nu_2}Q_{\nu_2\nu}$ to the reduced 2×2 Q -matrix, where the indices ν, ν' are in the dipole and octupole channels and the indices $\nu_{1,2}$ run over the modes with $J = 5, 7, \dots$. The calculation reveals both the dark state, where the dipole scattering is suppressed and the high- Q state stemming from the octupole modes. This high- Q (quasi-BIC) state is manifested as a sharp maximum in the octupole scattering channel, Fig. 3(c,d) for $r/h \approx 0.7$ (white dot). The dark state reveals itself as a dip in the dipole scattering channel, Fig. 3(a,b). An anticrossing between the dark state and the octupole resonance can be clearly seen by comparing the dip position with the frequency of the bare dark state, corresponding to decoupled dipole and octupole (dashed line). To summarize, our semi-analytical and numerical results for the linear scattering are in excellent agreement, confirming our interpretation of the high- Q state.

III. PHOTON PAIR GENERATION

Having established a theory of the high- Q state we will now utilize the spontaneous downconversion from this state to enhance the two-photon generation. The general expression for the quantum amplitude of the

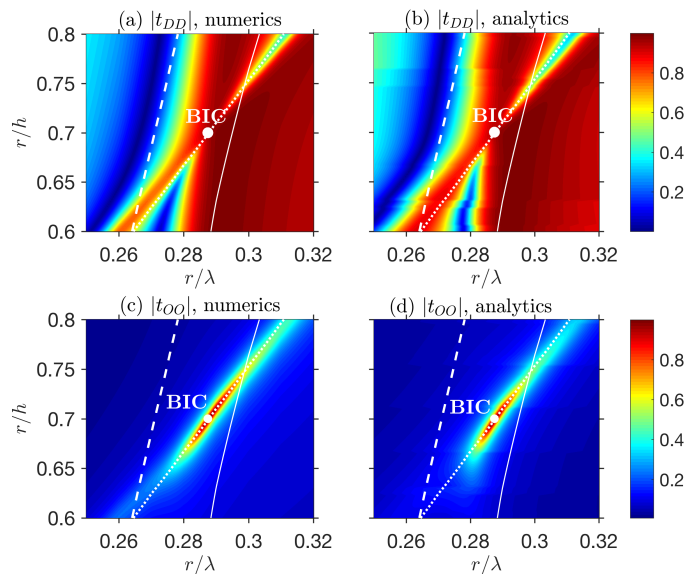


FIG. 3. Comparison of the scattering coefficients in numerical (a,c) and analytical (b,d) calculations. Top and bottom panels correspond to magnetic dipole and magnetic octupole scattering channels. Frequencies of the bare second magnetic dipole mode, dark dipole state and octupole mode, used in the analytical calculation, are plotted by solid, dotted and dashed lines, respectively. White dot indicates the high- Q (quasi-BIC) state. The disk permittivity is $\varepsilon = 10.73$.

two-photon generation in case of stationary excitation by the monochromatic pump $\mathbf{E}_p(\mathbf{r})$ at the frequency $\omega_p = \omega_i + \omega_s$ reads [19]

$$\psi(\mathbf{r}_i \alpha_i \omega_i; \mathbf{r}_s \alpha_s \omega_s) = \int d^3 r_0 G_{\alpha_i \alpha'_i}(\omega_i, \mathbf{r}_i, \mathbf{r}_0) \times G_{\alpha_s \alpha'_s}(\omega_s, \mathbf{r}_s, \mathbf{r}_0) \chi_{\alpha'_i \alpha'_s \gamma}^{(2)} E_p(\omega_p, \mathbf{r}_0), \quad (11)$$

where $\mathbf{r}_{i,s}$, $\alpha_{i,s}$, $\omega_{i,s}$ are the coordinates, polarizations and frequencies of idler and signal photons, respectively, $\chi^{(2)}$ is the nonlinear susceptibility tensor, and G is the electromagnetic Green function defined from $\text{rot rot } G = (\omega/c)^2 [\varepsilon(\mathbf{r})G + 4\pi\delta(\mathbf{r} - \mathbf{r}')]$. The Green function can be expressed in the basis of spherical harmonics as

$$G_{\alpha\beta}(\mathbf{r}, \mathbf{r}') = 4\pi i k_{\text{out}}^3 \sum_{\nu\nu'} [\overline{Q}^{-1}]_{\nu'\nu} (-1)^M \times [\mathbf{H}_\nu]_\alpha(k_{\text{out}}\mathbf{r}) [\overline{\mathbf{J}}_{\nu'}]_\beta(k_{\text{in}}\mathbf{r}'), \quad (12)$$

where the horizontal bar indicates the substitution $M \rightarrow -M, M' \rightarrow -M'$. Substituting Eq. (12) into Eq. (11) we obtain the following compact expression for the two-photon amplitude:

$$\psi(p \rightarrow \nu_s + \nu_i) = [\overline{Q}^{-1}]_{\nu'_s \nu_s}(\omega_s) [\overline{Q}^{-1}]_{\nu'_i \nu_i}(\omega_i) \times \langle \nu'_i, \nu'_s | \chi^{(2)} | \nu'_p \rangle [Q^{-1}]_{\nu'_p \nu_p}(\omega_p) a_{\nu_p}^{(0)}, \quad (13)$$

where $a_{\nu_p}^{(0)}$ are the multipolar expansion coefficients for the incident pump wave. The two-photon wavefunction is

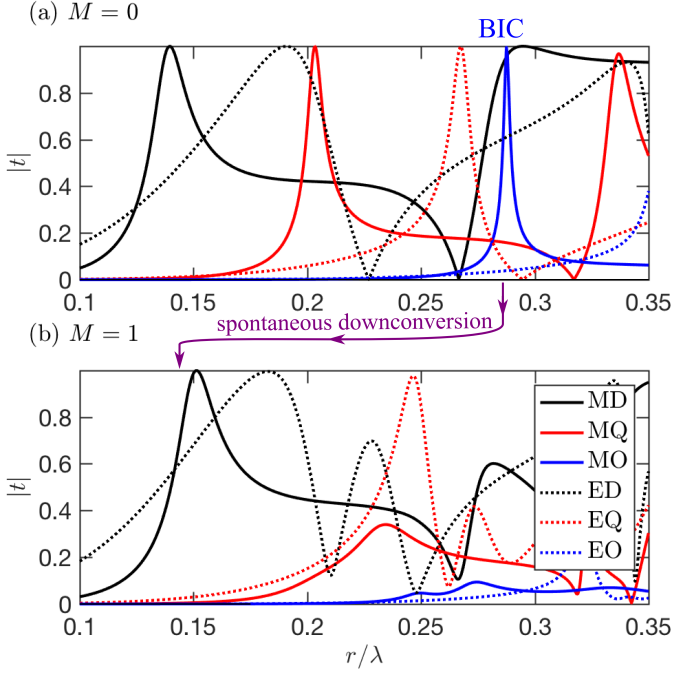


FIG. 4. (a,b) Multipolar decomposition of the linear scattering spectra in the channels with $M = 0$ (a) and $M = 1$ (b) for $r/h = 0.7$. The arrow indicates the process of generation of entangled electric (ED) and magnetic dipole (MD) modes due to the spontaneous decay of the high- Q quasi-BIC state at $r/\lambda \approx 0.29$ indicated in (a).

determined by the convolution of the inverted Q matrices at pump, signal and idler frequencies weighted by the matrix elements

$$\begin{aligned} \langle \nu'_i \nu'_s | \chi^{(2)} | \nu'_p \rangle &\equiv -(4\pi)^2 k_{i,\text{out}}^3 k_{s,\text{out}}^3 (-1)^{M_i + M_s} \\ &\times \chi_{\alpha\beta\gamma}^{(2)} \int_{(\text{disk})} d^3 r [\bar{\mathbf{J}}_{\nu'_i}]_{\alpha}(k_{i,\text{in}} \mathbf{r}) [\bar{\mathbf{J}}_{\nu'_s}]_{\beta}(k_{s,\text{in}} \mathbf{r}) [\mathbf{J}_{\nu'_p}]_{\gamma}(k_{p,\text{in}} \mathbf{r}) \end{aligned} \quad (14)$$

that describe their nonlinear coupling. Thus, the optical resonances of pump, signal and idler will be directly manifested in the two-photon count rate. Equation (13) rigorously incorporates the complex multipolar structure of the eigenmodes of the nanoparticle. It generalizes the results obtained in Ref. [25] in the point electric dipole approximation, applicable only to deeply subwavelength sizes.

The general symmetry properties of the integrals (14) will be discussed in our work Ref. [26] in more detail. Next, we consider the [001]-grown AlGaAs nanodisk, with the only independent component $\chi_{xyz}^{(2)} \neq 0$ [27]. The spontaneous decay process, relevant for the current study, and allowed by rotation and parity symmetry is

$$|\text{MD}_z\rangle \rightarrow |\text{ED}_x, \text{MD}_y\rangle + |\text{ED}_y, \text{MD}_x\rangle, \quad (15)$$

where MD and ED denote magnetic and electric dipole states with the corresponding polarization. As dis-

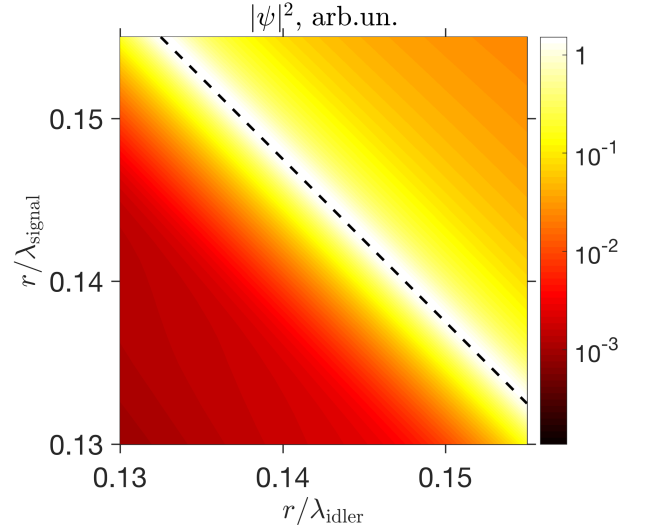


FIG. 5. (c) Square of the two-photon wavefunction depending on idler and signal photon energies. The detection is in the magnetic dipole, $M = 1$ and electric dipole, $M = 1$ signal and idler channels, respectively. Dashed line indicates the condition $r/\lambda_i + r/\lambda_s = 0.29$ of the resonance with the high- Q state. Calculated for $r/h = 0.7$.

cussed in the previous section, the MD_z channel has a high- Q -resonance due to the hybridization with the octupole mode. Hence, as soon as the incident pump wave excite the vertical magnetic dipole, it will couple to the high- Q -resonance and efficiently generate entangled signal and idler photons in the ED_x and MD_y channels. The linear scattering spectra for $r/h \approx 0.7$ and the an-

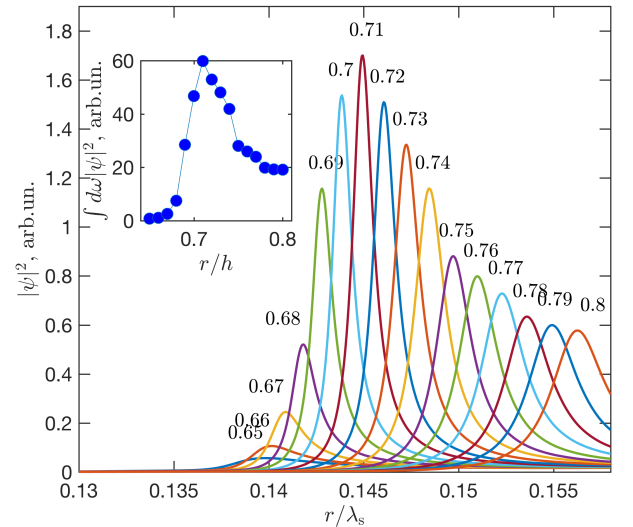


FIG. 6. Spectra of degenerate SPDC ($\lambda_i = \lambda_s = 2\lambda_p$) for different nanodisk aspect ratios r/h indicated near the corresponding curves. Inset shows the dependence of the area of the spectra on r/h . Other parameters are the same as in Fig. 5.

gular momentum projections $M = 0, 1$ are shown in Fig. 4(a,b), respectively. They confirm that the spontaneous parametric decay of the high- Q state at the frequency $r/\lambda \approx 0.3$ [Fig. 4(a)] will lead to the generation of the in-plane signal and idler electric and magnetic dipole modes with $r/\lambda \approx 0.15$ [Fig. 4(b)]. The relevant process is indicated by a violet arrow. In our calculation we excite the structure obliquely under the angle $\theta = 45^\circ$ from the z -axis by a TE-polarized plane wave. The resulting square of the two-photon wavefunction is shown in Fig. 5. It demonstrates a sharp maximum when the sum of signal and idler frequencies matches the high- Q state frequency, $r/\lambda_i + r/\lambda_s = 0.2875$ (see the dashed line). In order to further confirm that the maximum in SPDC is related to the formation of high- Q state we examine the dependence of the SPDC spectra on the nanodisk aspect ratio. Figure 6 presents the dependence of the degenerate SPDC with $\lambda_i = \lambda_s$ on r/h . The spectra feature a prominent maximum that becomes sharper and higher when the aspect ratio is tuned to the value $r/h = 0.71$. This is in full agreement with the formation of high- Q state in the linear scattering spectra, see Fig. 3. The asymmetry in the behavior on the peak maximum

with r/h traces the asymmetric profile of the MD mode at the pump frequency (black curve in Fig. 4a). The spectrally integrated degenerate SPDC efficiency increases near $r/h = 0.71$ as well, see the inset of Fig. 6.

IV. CONCLUSION

To conclude, we have proposed the high-quality states (quasi-bound states in continuum) in AlGaAs nanodisks for the spontaneous nonlinear generation of quantum-entangled photon pairs. Specifically, we have considered a process when the TE-polarized plane wave pump is obliquely incident at the frequency in the vicinity of the high- Q mode and the signal and idler photons are generated in the in-plane electric and magnetic dipole modes. For a certain aspect ratio of a disk, corresponding to the formation of high- Q -state, the generation of entangled pairs is resonantly enhanced. Our results are supported by rigorous full-wave numerical modeling, symmetry analysis and analytical theory, revealing the multipolar nature of the high- Q state.

-
- [1] J. W. Silverstone, D. Bonneau, K. Ohira, N. Suzuki, H. Yoshida, N. Iizuka, M. Ezaki, C. M. Natarajan, M. G. Tanner, R. H. Hadfield, V. Zwiller, G. D. Marshall, J. G. Rarity, J. L. O'Brien, and M. G. Thompson, "On-chip quantum interference between silicon photon-pair sources," *Nature Photonics* **8**, 104–108 (2013).
- [2] S. Wabnitz and B. J. Eggleton, *All-optical signal processing: data communication and storage applications*, Vol. 194 (Springer, 2015).
- [3] N. Somaschi, V. Giesz, L. D. Santis, J. C. Loredó, M. P. Almeida, G. Hornecker, S. L. Portalupi, T. Grange, C. Antón, J. Demory, C. Gómez, I. Sagnes, N. D. Lanzillotti-Kimura, A. Lemaître, A. Auffeves, A. G. White, L. Lanco, and P. Senellart, "Near-optimal single-photon sources in the solid state," *Nature Photonics* **10**, 340–345 (2016).
- [4] G. Reithmaier, M. Kaniber, F. Flassig, S. Lichtmanecker, K. Müller, A. Andrejew, J. Vučković, R. Gross, and J. J. Finley, "On-chip generation, routing, and detection of resonance fluorescence," *Nano Lett.* **15**, 5208–5213 (2015).
- [5] X. Guo, C. ling Zou, C. Schuck, H. Jung, R. Cheng, and H. X. Tang, "Parametric down-conversion photon-pair source on a nanophotonic chip," *Light: Science & Applications* **6**, e16249 (2016).
- [6] C. Wang, M. J. Burek, Z. Lin, H. A. Atikian, V. Venkataraman, I.-C. Huang, P. Stark, and M. Lončar, "Integrated high quality factor lithium niobate microdisk resonators," *Opt. Express* **22**, 30924–30933 (2014).
- [7] D. Smirnova and Y. S. Kivshar, "Multipolar nonlinear nanophotonics," *Optica* **3**, 1241–1255 (2016).
- [8] S. V. Makarov, M. I. Petrov, U. Zywiets, V. Milichko, D. Zuev, N. Lopanitsyna, A. Kuksin, I. Mukhin, G. Zograf, E. Ubyivovk, D. A. Smirnova, S. Starikov, B. N. Chichkov, and Y. S. Kivshar, "Efficient second-harmonic generation in nanocrystalline silicon nanoparticles," *Nano Lett.* **17**, 3047–3053 (2017).
- [9] D. Smirnova, A. I. Smirnov, and Y. S. Kivshar, "Multipolar second-harmonic generation by Mie-resonant dielectric nanoparticles," *Phys. Rev. A* **97**, 013807 (2018).
- [10] M. R. Shcherbakov, D. N. Neshev, B. Hopkins, A. S. Shorokhov, I. Staude, E. V. Melik-Gaykazyan, M. Decker, A. A. Ezhov, A. E. Miroshnichenko, I. Brener, A. A. Fedyanin, and Y. S. Kivshar, "Enhanced third-harmonic generation in silicon nanoparticles driven by magnetic response," *Nano Lett.* **14**, 6488–6492 (2014).
- [11] R. Camacho-Morales, M. Rahmani, S. Kruk, L. Wang, L. Xu, D. A. Smirnova, A. S. Solntsev, A. Miroshnichenko, H. H. Tan, F. Karouta, S. Naureen, K. Vora, L. Carletti, C. De Angelis, C. Jagadish, Y. S. Kivshar, and D. N. Neshev, "Nonlinear generation of vector beams from AlGaAs nanoantennas," *Nano Lett.* **16**, 7191–7197 (2016).
- [12] D. A. Smirnova, A. B. Khanikaev, L. A. Smirnov, and Y. S. Kivshar, "Multipolar third-harmonic generation driven by optically induced magnetic resonances," *ACS Photonics* **3**, 1468–1476 (2016).
- [13] G. Marino, A. S. Solntsev, L. Xu, V. F. Gili, L. Carletti, A. N. Poddubny, M. Rahmani, D. A. Smirnova, H. Chen, G. Zhang, A. V. Zayats, C. D. Angelis, G. Leo, Y. S. Kivshar, A. A. Sukhorukov, and D. N. Neshev, in preparation.
- [14] G. Marino, A. S. Solntsev, L. Xu, V. F. Gili, L. Carletti, A. N. Poddubny, M. Rahmani, D. Smirnova, H. Chen, G. Zhang, A. V. Zayats, C. D. Angelis, G. Leo, Y. S. Kivshar, A. A. Sukhorukov, and D. N. Neshev, "Sum-frequency- and photon-pair-generation in AlGaAs nano-disks," in *Advanced Photonics 2018 (BGPP, IPR,*

- NP, NOMA, Sensors, Networks, SPCom, SOF*) (OSA, 2018).
- [15] L. Carletti, K. Koshelev, C. De Angelis, and Y. Kivshar, “Giant nonlinear response at the nanoscale driven by bound states in the continuum,” *Phys. Rev. Lett.* **121**, 033903 (2018).
- [16] C. W. Hsu, B. Zhen, A. D. Stone, J. D. Joannopoulos, and M. Soljačić, “Bound states in the continuum,” *Nature Reviews Materials* **1**, 16048 (2016).
- [17] M. V. Rybin, K. L. Koshelev, Z. F. Sadrieva, K. B. Samusev, A. A. Bogdanov, M. F. Limonov, and Y. S. Kivshar, “High- q supercavity modes in subwavelength dielectric resonators,” *Phys. Rev. Lett.* **119**, 243901 (2017).
- [18] A. A. Bogdanov, K. L. Koshelev, P. V. Kapitanova, M. V. Rybin, S. A. Gladyshev, Z. F. Sadrieva, K. B. Samusev, Y. S. Kivshar, and M. F. Limonov, “A direct link between Fano resonances and bound states in the continuum,” ArXiv e-prints (2018), [arXiv:1805.09265](https://arxiv.org/abs/1805.09265) [[physics.optics](https://arxiv.org/abs/1805.09265)].
- [19] A. N. Poddubny, I. V. Iorsh, and A. A. Sukhorukov, “Generation of photon-plasmon quantum states in nonlinear hyperbolic metamaterials,” *Phys. Rev. Lett.* **117**, 123901 (2016).
- [20] F. Lenzini, A. N. Poddubny, J. Titchener, P. Fisher, A. Boes, S. Kasture, B. Haylock, M. Villa, A. Mitchell, A. S. Solntsev, A. A. Sukhorukov, and M. Lobino, “Direct characterization of a nonlinear photonic circuit’s wave function with laser light,” *Light: Science & Applications* **7**, 17143 (2018).
- [21] P. C. Waterman, “Symmetry, Unitarity, and Geometry in Electromagnetic Scattering,” *Phys. Rev. D* **3**, 825–839 (1971).
- [22] L. Tsang, J. Kong, and K. Ding, *Scattering of electromagnetic waves: Theories and applications*, Wiley series in remote sensing (J. Wiley, 2000).
- [23] M. I. Mishchenko, L. D. Travis, and A. A. Lacis, *Scattering, absorption, and emission of light by small particles* (Cambridge university press, 2002).
- [24] C. W. Hsu, B. G. DeLacy, S. G. Johnson, J. D. Joannopoulos, and M. Soljačić, “Theoretical criteria for scattering dark states in nanostructured particles,” *Nano Lett.* **14**, 2783–2788 (2014).
- [25] N. A. Olekhno, M. I. Petrov, and I. V. Iorsh, “Spontaneous parametric downconversion of light by a dielectric nanoparticle,” *J. Phys: Conf. Ser.* **993**, 012022 (2018).
- [26] K. Frizyuk, D. Smirnova, I. Volkovskaya, A. Poddubny, and M. Petrov, “Second-harmonic generation in Mie-resonant dielectric nanoparticles made of noncentrosymmetric materials,” in preparation.
- [27] R. W. Boyd, *Nonlinear optics* (Academic press, 2003).